# CHAPTER 5

# FRINGE ANALYSIS & PHASE STEPPING INTERFEROMETRY

*"Wo viel Licht ist, ist starker Schatten."*
*("Where there is much light, the shadows are deepest")*
*Goethe*

## 5.1 ANALYSIS OF INTERFERENCE FRINGES

### 5.1.1 Introduction to interference fringe analysis

Using interferometry it is possible to compare measured and reference wavefronts to a high degree of accuracy. Interferometric measurement techniques such as holographic interferometry, speckle interferometry, moiré *etc.* have found many applications from the measurement of engine blocks [**1**], hip joint prosthesis design [**2**] to high accuracy measurement of optical components such as mirrors, flats and lenses.

To achieve these accuracies it is necessary to use computer evaluation of the interference fringes. Image processing can be used to enhance the fringe patterns and remove noise before the phase is evaluated. Post-processing of the data often includes finite element analysis or boundary element analysis techniques to solve specific application problems.

Each technique requires determination of the interference phase at a number of points in the field to generate a phase distribution or phase map. There are many techniques for phase extraction, each suited to a particular experimental design. These techniques are: fringe skeletonisation, phase-shifting, phase-stepping, Fourier transform, temporal heterodyning, spatial heterodyning (carrier frequency) and phase locking. There are excellent review articles which deal with the variety of techniques used [**3**,**4**,**5**,**6**,**7**,**8**].

At its most simple level, fringe analysis can be performed by eye. In the Twyman-Green interferometer shown in figure 5.1, interference fringes are produced on a surface or optical component to be tested. The fringes are detected by a CCD array and displayed on a monitor. The equation for the intensity of the fringes in the plane of the detector array is

$$I(x,y,t) = a(x,y) + b(x,y)\cos\left[\phi(x,y) + \Phi_R(x,y,t)\right] \tag{5.1}$$

Here, *a(x,y)* represents the variation of the background illumination, *b(x,y)* describes the noise and contrast variations, $\phi(x,y)$ is related to the surface to be measured and $\Phi_R(x,y,t)$ is the reference phase, or wavefront at time *t.* The co-sinusoidal variation of *I* leads to a set of interference fringes, of co-sinusoidal intensity.

The fringes can be regarded as contour lines of surface height of the test object, spaced at intervals of $\lambda/2$ where $\lambda$ is the wavelength of the light source. Using these fringes as contours, one can determine by eye, wavefront aberrations or surface defects to about $\lambda/5$ or $\lambda/10$, simply by observing the positions of the fringes in the interferogram. It is easy to detect defects such as spherical aberration, coma, or to spot inhomogeneities in refractive components, or flatness errors in mirrors.

For more accurate measurement, it is necessary to be able to sub-divide the fringes, *i.e.* to measure the phase at all points in the display. This requires some computer processing of the intensity distribution in the image.

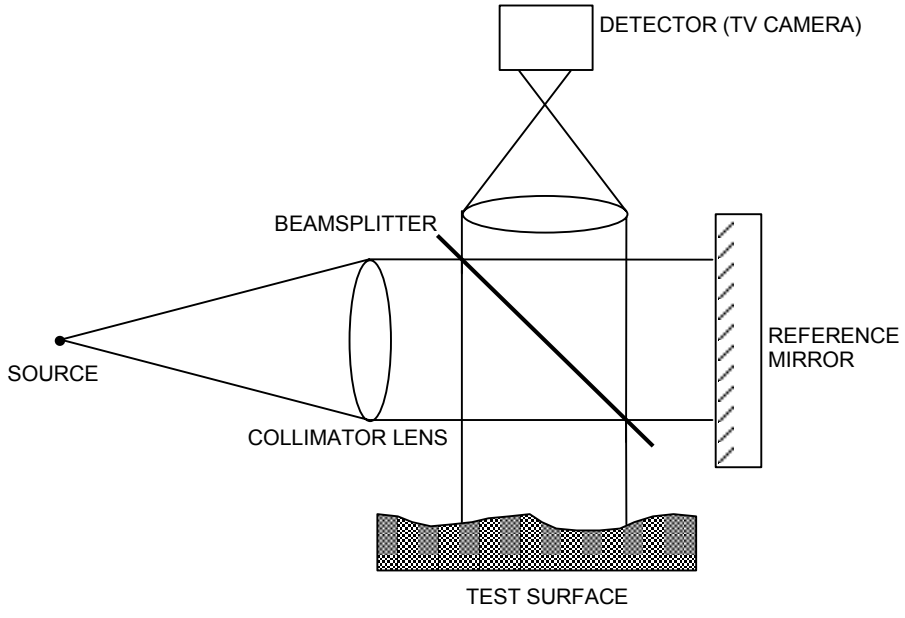


***Figure 5.1*** *- Example Twyman-Green interferometer for optical testing*

### 5.1.2 Fringe skeletonisation methods

Fringe skeletonisation is an extension of the fringe analysis performed by eye based on tracking fringe maxima or minima across the field. The computer algorithm searches for maxima and minima in the digitised interference pattern [**9**]. The phase at these points corresponds to multiples of $\pi$. Many algorithms exist for tracking along a fringe extremum, usually based on finding the normal to the maximum gradient of the intensity, or by following a path of minimum change of intensity. The result is a set of lines, one pixel wide, which correspond to the extrema, and are often overlaid on the original image for comparison. The analysis then requires the joining together of lines which are disconnected (such as near a defect) followed by numbering of the lines. This last step must usually be performed with user input, especially where lines are discontinuous [**10**]. The phase at points lying between fringe extrema is calculated by linear, polynomial or spline interpolation along a suitable direction in the phase map.

The main advantage of fringe skeletonisation is that it requires only one digitised interferogram and so temporal drifts of the experimental arrangement have little effect on the phase measurement. However, the accuracy is approximately *λ/10*, the computation time is long, there is no averaging between many frames to suppress noise and it is sometimes difficult to assign the correct sign to phase gradients, since the intensity change can appear the same for both positive and negative gradients.

### 5.1.3 Fourier transform methods

The Fourier transform technique requires only one interference pattern, for which the reference phase, $\Phi_R(x,y,t)$ can be arbitrarily set to zero. Expanding the cosine function in (5.1) using Euler's formula, and the definition

$$c(x,y) = \frac{1}{2} b(x,y) e^{i\phi(x,y)} \tag{5.2}$$

gives

$$I(x,y) = a(x,y) + c(x,y) + c^*(x,y) \tag{5.3}$$

Applying the two-dimensional Fourier transform to this gives

$$\boldsymbol{I}(u,v) = \boldsymbol{A}(u,v) + \boldsymbol{C}(u,v) + \boldsymbol{C}^*(u,v) \tag{5.4}$$

Since *I(x,y)* is real in the spatial domain, it follows that $\boldsymbol{I}(u,v)$ is Hermitian in the spatial frequency domain, *i.e.* $\Re\{\boldsymbol{I}(u,v)\}$ is even and $\Im\{\boldsymbol{I}(u,v)\}$ is odd. The amplitude spectrum is symmetric about the zero-frequency position, and so $\boldsymbol{C}(u,v)$ and $\boldsymbol{C}^*(u,v)$ contain the same information. By bandpass filtering in the spatial frequency domain, $\boldsymbol{A}(u,v)$ and $\boldsymbol{C}^*(u,v)$ can be removed to leave $\boldsymbol{C}(u,v)$, which when the inverse Fourier transform is applied gives *c(x,y)* which is now complex. The phase can then be measured from

$$\phi(x,y) = \arctan\frac{\Im\{c(x,y)\}}{\Re\{c(x,y)\}} \tag{5.5}$$

In effect, the Fourier transform method is a least squares fit of a linear combination of harmonic functions to the interference pattern.

If only one interferogram is used in the evaluation of the phase, then there is an ambiguity in the sign of the phase, due to loss of information during the filtering stage. This can be resolved by using a second interferogram with the reference phase shifted by up to $\pi$.

### 5.1.4 Temporal heterodyning methods

In temporal heterodyning, the two interfering wavefronts are formed from sources which have different frequencies, approximately a few kHz apart [**11**]. A common technique for generating these frequencies is to split a laser output into two modes by magnetic (Zeeman) splitting. The interferogram oscillates at the frequency of the beat between the two waves. A photodetector is used to sample the signal at points in the interferogram (there are no CCD detector arrays with high enough bandwidths). The phase can be measured either as the difference in phase between two detector points or between a single point and a reference phase signal. Phase distributions can only be measured by scanning the detector in the image.

### 5.1.5 Spatial heterodyning methods

To perform spatial heterodyne interferometry with frequency domain processing, a system used for Fourier transform interferometry has an additional set of carrier fringes introduced by tilting a mirror. These heterodyne carrier fringes have spatial frequency $f_0$. The carrier frequency will cause a phase gradient across the image of size $2\pi f_0 x$. This then takes the place of $\Phi_R(x,y,t)$ in equation (5.1). This carrier frequency is removed by shifting the filtered spectral components in the frequency domain. This

allows the two components $\boldsymbol{C}(u,v)$ and $\boldsymbol{C}^*(u,v)$ to be effectively separated, making the filtering operation easier to perform. In effect, the single interferogram can be regarded as a multi-channel interferogram, where the different channels are separated spatially, *i.e.* in different pixels in the image, rather that at the same pixels, but separated in time, as in temporal techniques.

Another version of spatial heterodyning uses pointwise multiplication of the digitised intensity data by $\cos(2\pi f_0 x)$ and $\sin(2\pi f_0 x)$ to analyse the data in the spatial domain. If the spatial frequency of the fringes is similar to the frequency of these additional quadrature terms, then low frequency difference components can be separated by a low pass filter. These components are in phase quadrature in terms of the phase to be measured.

The technique of spatial heterodyning requires superposition of fringes (either real or in software) of a similar spatial frequency to the original interferometric fringes. This may not be possible where the original fringes are not of equal inclination and spacing. The technique using extra tilting of the mirror requires that the phase and amplitude of the wave to be measured must not change appreciably within the period of the spatial-carrier-frequency [**12**], *i.e.* the surface to be measured must be flat or a large tilt must be given to produce many fringes across the surface.

### 5.1.6 Phase locking methods

In the phase locking technique, the phase of the reference beam is modulated sinusoidally by less than $\lambda/2$, at a frequency $\omega$. A bandpass filter centred at $\omega$ is used to sample the intensity at each point in the interferogram. At points where $\phi(x,y) = N\pi$ the detected intensity averages to zero. Thus the phase lock technique is a dynamic method of fringe skeletonisation, in real time. The technique has the same disadvantages as that of fringe skeletonisation.

### 5.1.7 Summary of phase measurement methods

Table 5.1 shows a summary of the phase measurement methods examined so far as well as the technique of phase-stepping interferometry, which will be examined shortly. Whether one technique is better than another depends on the application.

| | Fringe skeleton | Phase stepping | Fourier transform | Temporal heterodyne | Spatial heterodyne | Phase locking |
|---|---|---|---|---|---|---|
| No. of images | 1 | 3,4,5 | 1(2) | 1 per pixel | 1 | 1 |
| Resolution (λ) | 1 - 0.1 | 0.1 - 0.001 | 0.1 - 0.03 | 0.01 - 0.001 | 0.1 - 0.03 | 1 - 0.1 |
| Measurement at all points | no | yes | yes | yes | yes | no |
| Noise suppression | partial | yes | yes | partial | yes | partial |
| Sign detection | no | yes | no(yes) | yes | (yes) | no |
| Difficulty | low | high | low | very high | low | medium |
| Computation time | long | short | long | very long | very long | long |
| Real time | some | some | no | some | no | yes |

***Table 5.1*** *- Summary of phase measurement techniques*

## 5.2 PHASE-STEPPING INTERFEROMETRY (PSI)

### 5.2.1 History of PSI

Phase-measuring, Phase-Shifting or Phase-Stepping Interferometry is a technique used in the analysis of interference patterns generated by multiple beam interferometry. PSI has existed in its basic form for less than 3 decades, and may be regarded as temporal multiplexing of the interferograms to be analysed (temporal-carrier) where the use of an extra time variable reduces the problem of phase extraction to reading the phase of a sinusoidal signal, with varying time co-ordinate, but fixed spatial co-ordinates [**13**,**14**,**15**,**16**,**17**,**18**,**19**].

There has been a resurgence of interest in PSI as a measurement technique since the mid 1980s. This has been due to recent advances in the equipment required in PSI for image detection and processing, together with a general reduction in cost of computer power. Also, there has been a trend for measurement instruments and systems to become more automated and objective in their analyses - PSI is ideal for this, as it is easily implemented on standard ranges of computers.

### 5.2.2 Basic theory of PSI

PSI, as its name suggests, involves the variation of phase within the interferometer, by a controlled amount. All designs of phase-stepping interferometers have a number of features in common:

(i) The interferogram is imaged onto a detector *e.g.* CCD TV camera, photodiode array, holographic plate

(ii) The interferogram is a comparison between the wavefronts generated by test and reference surfaces

(iii) The relative phase of one of the interferometer arms (reference or test) is varied with respect to the other by a fixed and known amount, either continuously (phase-shifting) or in discrete steps (phase-stepping)

(iv) The intensity of the interferogram is either summed continuously or stored at each step, depending on which method is used in (iii)

(v) After the phase-stepping or shifting is complete, the analysis of the stored data is undertaken. A major advantage of phase-stepping interferometry is that a detector array such as a CCD camera can be used to make measurements simultaneously at a very large number of points covering the interference pattern, the resolution being limited by the optical magnification and the detector pixel size.

### 5.2.3 Derivation of generic PSI equations

The phase calculation of PSI is based on the fact that the intensity $I(x,y)$ at a point $(x,y)$ in the interferogram is the result of interference of two wavefronts. Considering the Twyman-Green interferometer shown in figure 5.2, which is assumed to be made from optically perfect components, *i.e.* there are no aberrations.

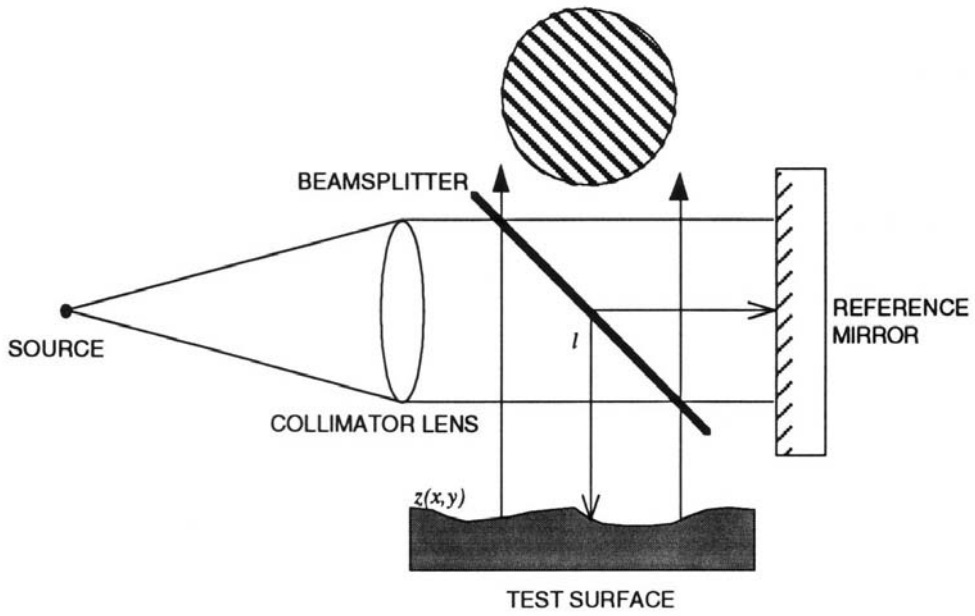


***Figure 5.2*** *- Idealised interferometer for testing surfaces*

In figure 5.2 and the following derivation, *z(x,y)* is the surface profile of the object under test, $\lambda$ is the wavelength of the monochromatic light, *l* is representative of the total (average) optical path difference between the two surfaces. Wavefronts from the reference and test arms are given respectively by

$$w_r = ae^{2ikl} \tag{5.5}$$

$$w_t = be^{2ikz(x,y)} \tag{5.6}$$

with $k = 2\pi/\lambda$ and *a* and *b* are the amplitudes of the interfering wavefronts, due to different reflectivities of the surfaces. In the interference pattern,

$$I(x,y,l) = (w_r + w_t)(w_r + w_t)^* \tag{5.7}$$

$$= a^2 + b^2 + 2ab\cos(2k(z(x,y) - l)) \tag{5.8}$$

The term $(a^2 + b^2)$ represents the background intensity, or DC level, and the variation of $2ab\cos(2k(z(x,y) - l))$ represents the interference fringes, observed as co-sinusoidal variations in intensity, *I(x,y,l)*. One can vary the intensity *I(x,y,l)* either by keeping *l* constant, and changing *x* or *y* - *i.e.* moving across a non-flat surface, or by keeping *x* and *y* constant and varying *l*, the optical path difference. In PSI, *l* is varied by varying the phase of one of the beams, *e.g.* by moving the reference mirror longitudinally along the beam axis. As the value of *l* is varied, the intensity *I(x,y,l)* at each point *(x,y)* in the interferogram varies in a co-sinusoidal manner (assuming linear detection, non-

aberrated optics *etc*). The premise of PSI is that by knowing the variation in *l,* and observing the variation in *I(x,y,l)* at each point in the interferogram, one can correlate the two, and hence retrieve *z(x,y)* in terms of *k* (or $\lambda$).

This can be seen by re-writing (5.8):

$$I(x,y,l) = a_0 + a_1 \cos 2kl + b_1 \sin 2kl \tag{5.9}$$

where $a_1$ and $b_1$ are functions of *x* and *y*, and hence contain information about *z(x,y)*. Now if the phase in one beam is stepped (by varying *l*) in *n* steps, each of which is *1/n* of a fringe *i.e.* $\lambda/2n$ in size, then, using the orthogonality relationships for sin and cos

$$a_0 = \frac{1}{n}\sum_{i=1}^{n} I(x,y,l_i) = a^2 + b^2 \tag{5.10}$$

$$a_1 = \frac{2}{n}\sum_{i=1}^{n} I(x,y,l_i)\cos 2kl_i = 2ab\cos(2kz(x,y)) \tag{5.11}$$

$$b_1 = \frac{2}{n}\sum_{i=1}^{n} I(x,y,l_i)\sin 2kl_i = 2ab\sin(2kz(x,y)) \tag{5.12}$$

from which

$$\frac{b_1}{a_1} = \frac{\frac{2}{n}\sum_{i=1}^{n} I(x,y,l_i)\sin 2kl_i}{\frac{2}{n}\sum_{i=1}^{n} I(x,y,l_i)\cos 2kl_i} = \frac{2ab\sin(2kz(x,y))}{2ab\cos(2kz(x,y))} \tag{5.13}$$

$$= \tan(2kz(x,y)) \tag{5.14}$$

$$\therefore\ 2kz(x,y) = \arctan\left(\frac{b_1}{a_1}\right) \tag{5.15}$$

$$\therefore\ z(x,y) = \frac{1}{2k}\arctan\left(\frac{b_1}{a_1}\right) \tag{5.16}$$

*i.e. z(x,y)* can be determined (to within modulo $2\pi$) from $a_1$ and $b_1$, the summed intensities at *(x,y)*. This is the basis of PSI. There are many variations of this basic equation, which are detailed in § 5.3.

### 5.2.4 Typical applications of PSI

PSI has been widely used [**14**,**20**,**21**] in the testing of optical components [**22**,**23**]. The range of surface variation measurable by basic PSI is limited to a few microns. This is due to the compromise between having lots of fringes across the interferogram either as the result of tilt or due to large test surface deviations, and the requirement that each fringe must be large enough in width to be imaged onto at least 2 detector pixels. If the fringe is smaller than 2 pixels, each pixel will integrate the intensity of the whole fringe, and no fringe modulation will be observed during phase stepping. Another requirement of these techniques is that the surface under test is smooth and has no discontinuities present of magnitude greater than the measurement wavelength, as these discontinuities cannot be distinguished from the $2\pi$ discontinuities present in the wrapped phase data.

### 5.2.5 Phase variation methods for PSI

In general, any technique which varies the phase in one or more of the interferometer beams can be used in PSI. The most common techniques include: moving diffraction gratings [**24**], moving the reference mirror by use of a PZT, the Bragg effect in an acousto-optic modulator [**25**] and rotating a half-wave plate in a polarised interferometer [**24**,**26**].

## 5.3 PHASE STEPPING TECHNIQUES

### 5.3.1 Basic phase-stepping techniques

Let the system of fringes in an interferometer have visibility $V$ which is defined as

$$V = \frac{I_{\max} - I_{\min}}{I_{\max} + I_{\min}} \tag{5.17}$$

The mean intensity of the two beams is $I_0$. When the phase of the reference beam is $\Phi$, the intensity at a point in the interferogram will be given by

$$I_r = I_0 + I_0 V \cos(\Phi - \phi) \tag{5.18}$$

Taking the expression

$$I(x,y) = I_0\big(1 + V(x,y)\cos(\Phi - \phi(x,y))\big) \tag{5.19}$$

and using

$$\cos(A - B) = \cos A \cos B + \sin A \sin B$$

gives

$$I(x,y) = I_0 + I_0 V \cos\phi(x,y)\cos\Phi + I_0 V \sin\phi(x,y)\sin\Phi \tag{5.20}$$

Now using phase stepping, *i.e.* picking discrete values $\Phi_r$ of $\Phi$ given by

$$\Phi_r = \frac{(r-1)2\pi}{R} \qquad \text{with } r = 1,2,\ldots,R \tag{5.21}$$

the intensity at a particular point $(x,y)$ in the interferogram will be given by

$$I_r = I_0 + I_0 V \cos(\Phi_r - \phi) \tag{5.22}$$

expanding this gives

$$I_r = I_0 + I_0 V \cos\Phi_r \cos\phi + I_0 V \sin\Phi_r \sin\phi \tag{5.23}$$

Multiplying (5.23) by $\cos\Phi_r$ and $\sin\Phi_r$ separately gives

$$I_r \cos\Phi_r = I_0 \cos\Phi_r + I_0 V \cos\phi \cos^2\Phi_r + I_0 V \sin\phi \sin\Phi_r \cos\Phi_r \tag{5.24}$$

$$I_r \sin\Phi_r = I_0 \sin\Phi_r + I_0 V \cos\phi \cos\Phi_r \sin\Phi_r + I_0 V \sin\phi \sin^2\Phi_r \tag{5.25}$$

Now summing equations (5.23) to (5.25) over $r$

$$\sum_{r=1}^{R} I_r = \sum_{r=1}^{R} I_0 + \sum_{r=1}^{R} I_0 V \cos\Phi_r \cos\phi + \sum_{r=1}^{R} I_0 V \sin\Phi_r \sin\phi \tag{5.26}$$

$$\sum_{r=1}^{R} I_r \cos\Phi_r = \sum_{r=1}^{R} I_0 \cos\Phi_r + \sum_{r=1}^{R} I_0 V \cos\phi \cos^2\Phi_r + \sum_{r=1}^{R} I_0 V \sin\phi \sin\Phi_r \cos\Phi_r \tag{5.27}$$

$$\sum_{r=1}^{R} I_r \sin\Phi_r = \sum_{r=1}^{R} I_0 \sin\Phi_r + \sum_{r=1}^{R} I_0 V \cos\phi \cos\Phi_r \sin\Phi_r + \sum_{r=1}^{R} I_0 V \sin\phi \sin^2\Phi_r \tag{5.28}$$

Now using the orthogonality relationships for sin and cos:

$$\sum_x^{2\pi} \sin(mx)\sin(nx) = \begin{Bmatrix} 0 & \forall & m \neq n \\ \pi & \forall & m = n \neq 0 \end{Bmatrix}$$

$$\sum_x^{2\pi} \cos(mx)\cos(nx) = \begin{Bmatrix} 0 & \forall & m \neq n \\ \pi & \forall & m = n \neq 0 \end{Bmatrix}$$

$$\sum_x^{2\pi} \cos(mx)\sin(nx) = 0 \quad \forall \quad m,n$$

then equations (5.26) to (5.28) reduce to

$$\sum_{r=1}^{R} I_r = RI_0 \tag{5.29}$$

$$\sum_{r=1}^{R} I_r \cos\Phi_r = \frac{1}{2} RI_0 V \cos\phi \tag{5.30}$$

$$\sum_{r=1}^{R} I_r \sin\Phi_r = \frac{1}{2} RI_0 V \sin\phi \tag{5.31}$$

from which it follows that

$$\frac{2\sum_{r=1}^{R} I_r \sin\Phi_r}{2\sum_{r=1}^{R} I_r \cos\Phi_r} = \frac{RI_0 \sin\phi}{RI_0 \cos\phi} \tag{5.32}$$

and hence

$$\boxed{\tan\phi = \frac{\sum_{r=1}^{R} I_r \sin\Phi_r}{\sum_{r=1}^{R} I_r \cos\Phi_r}} \tag{5.33}$$

This is the basic equation for all multi-step phase-stepping techniques.

### 5.3.2 Phase-shifting interferometry

There is another form of phase-measuring interferometry, phase-shifting interferometry. Here the phase is continuously varied and the detector integrates the intensity at each point over a range of phases. Grievenkamp [**27**] shows the integrated intensity to be

$$I_i(x,y) = \frac{1}{\Delta}\int_{x_i-\Delta/2}^{x_i+\Delta/2} I_0(x,y)\{1+\gamma_0\cos[\phi(x,y)+\alpha(t)]\}d\alpha(t) \qquad (5.34)$$

$I_0(x,y)$ is the average intensity at detector point *(x,y)*, $\gamma_0$ is the modulation of the fringe pattern (corresponds to *V* used above), $\alpha_i$ is the average value of the relative phase shift for the i$^{th}$ exposure, $\phi(x,y)$ is the test wavefront phase to be determined, and $\Delta$ is the phase shift over which the intensities are summed.

Thus

$$I_i(x,y) = I_0(x,y)\{1+\gamma_0\,\mathrm{sinc}(\Delta/2)\cos[\phi(x,y)+\alpha_i]\}$$

Substituting $\Delta = 0$ (integrating over zero phase range), the above equation reduces to the phase-stepping case. The phase-shifting technique is often referred to as the 'Integrating Bucket' approach.

### 5.3.3 Four quadrant arctangent routine

The basic phase-stepping or phase-shifting equations have an initial limitation. Simply applying an equation of the form

$$\phi = \arctan\left(\frac{a}{b}\right)$$

returns values of $\phi$ in the range $-\pi/2$ to $\pi/2$ *i.e.* a range of $\pi$. This is unsatisfactory as each interference fringe corresponds to a range of phase values over the range 0 to $2\pi$ . This is easily resolved by noting that *a* corresponds to a sinusoid and *b* to a co-sinusoid, and thus the signs (+ or - ) of these quantities can be used to uniquely define a quadrant for each calculation of $\phi$, based on the four possible combinations.

| a | b | $\phi$ |
|---|---|---|
| + | + | $\phi$ |
| + | - | $\pi-\phi$ |
| - | + | $2\pi-\phi$ |
| - | - | $\pi+\phi$ |

***Table 5.2*** *- Four-quadrant lookup table*

Suitable adjustments are made when either *a* or *b* or both are zero. Thus by use of a PSI technique based around equation (5.33), followed by application of a 4-quadrant arctangent, the relative phase at each point in the interferogram can be determined modulo $2\pi$.

### 5.3.4 Two position phase-stepping technique

A two position technique has been used by Santoyo *et al* [**28**] in the analysis of Electronic Speckle Pattern Interference, where the fringes are defined by a different equation to that of conventional interferometry. It is not suitable for general PSI, as with only two measurements, $I_1$ and $I_2$, it is not possible to solve for all three variables of the general PSI equation. However the technique is suited to the analysis of speckle pattern interferograms, as these are of the form

$$I(x,y) \propto \sin(\theta + \Delta\phi / 2) \tag{5.35}$$

where $\Delta\phi$ is the phase change due to surface deformation, and $\theta$ is the relative phase between the 2 beams. Hence with 2 values of $\theta$, separated by $\pi/2$,

$$\frac{I_2}{I_1} \propto \frac{\sin(\theta + \Delta\phi/2)\sin(\Delta\phi/2)}{(\theta + \Delta\phi/2 + \pi/2)\sin(\Delta\phi/2)} \tag{5.36}$$

$$\frac{\sin(\theta + \Delta\phi/2)}{\cos(\theta + \Delta\phi/2)}$$

$$\tan(\theta + \Delta\phi/2)$$

Hence knowing $\theta$ to be constant, one can determine $\Delta\phi$ for a deformation.

The initial frames are first processed to improve contrast, and then the phase calculation is performed using

$$\phi(x,y) = \arctan\left(\frac{I_2(x,y)}{I_1(x,y)}\right) \tag{5.37}$$

Processing is carried out using a four-quadrant arctan lookup table using sign information about $I_1$ and $I_2$ to resolve quadrant ambiguities. However the method requires that the phase step $\theta$ be exactly $\pi/2$, otherwise the calculated value of $\phi$ will be incorrect.

### 5.3.5 Three position phase-stepping technique

As mentioned above, a minimum of three sets of recorded intensity data are required to solve the PSI equation (5.8). A common 3 position technique uses phase steps of $\pi/2$, using relative phases of $\pi/4$, $3\pi/4$, $5\pi/4$. Under these conditions the following analysis can be applied for all points $(x,y)$.

$$\begin{aligned} I_1 &= I_0 + I_0\gamma\cos(\phi + \pi/4) \\ I_2 &= I_0 + I_0\gamma\cos(\phi + 3\pi/4) \\ I_3 &= I_0 + I_0\gamma\cos(\phi + 5\pi/4) \end{aligned} \tag{5.38}$$

from which it can be shown that

$$\phi = \arctan\left(\frac{I_3 - I_2}{I_1 - I_2}\right) \tag{5.39}$$

Other variations in the three position technique use a phase shift of $2\pi/3$ between each image, for which the phase is calculated from

$$\phi = \arctan\left(\sqrt{3}\frac{I_3 - I_2}{2I_1 - I_2 - I_3}\right) \tag{5.40}$$

However this technique takes longer to perform the phase calculation as there are more terms.

The three-position technique is subject to the same basic error sources as the four-position technique, and analysis of the errors will be dealt with simultaneously in § 5.3.7 for comparison.

### 5.3.6 Four position phase-stepping technique

Although only 3 images are required to solve for the three variables of the PSI equation, in practice more than 3 images are often digitised for ease of computation, noise suppression and reduction in sensitivity to phase stepper errors. In the four position technique, the nominal phase-step is $\pi/2$, and the reference phase takes values of 0, $\pi/2$, $\pi$, and $3\pi/2$. Using these values, the intensities at each point in images 1 to 4 are

$$\begin{aligned} I_1 &= I_0 + I_0\gamma\cos(\phi) \\ I_2 &= I_0 + I_0\gamma\cos(\phi + \pi/2) &&= I_0 - I_0\gamma\sin(\phi) \\ I_3 &= I_0 + I_0\gamma\cos(\phi + \pi) &&= I_0 - I_0\gamma\cos(\phi) \\ I_4 &= I_0 + I_0\gamma\cos(\phi + 3\pi/2) &&= I_0 + I_0\gamma\sin(\phi) \end{aligned} \tag{5.41}$$

from which

$$\phi = \arctan\left(\frac{I_4 - I_2}{I_1 - I_3}\right)$$

As expected, due to the averaging over more images in the four position technique, it has a lower error than the three position technique, although it requires more storage and takes longer to process the images to extract the phase.

### 5.3.7 Errors for three and four position techniques

#### 5.3.7.1 Error due to phase stepper error

The principal error which affects most PSI technique is that of phase-stepper error. The techniques of PSI assume a fixed and known phase step size, which for the 3 and 4 position techniques is $\pi/2$. However non-linearities in the movement of a PZT performing the phase-stepping, or a mis-calibration of phase step size can cause the calculated phase to be in error. A general equation for the error in the phase map due to the phase step error can be derived as follows.

The following analysis is assumed to apply to every point $(x,y)$ in the interferogram.

Assuming an error $\varepsilon_r$ in the size of the phase step, *i.e.*

$$\Phi'_r = \Phi_r + \varepsilon_r \tag{5.42}$$

where $\Phi'_r$ is the achieved phase step, and $\Phi_r$ is the correct phase step. Using

$$I_r = I_0 + I_0 \gamma \cos(\phi - \Phi_r) \tag{5.43}$$

as an equation for the intensity at a point for phase step angle $\Phi_r$,

$$I'_r = I_0 + I_0 \gamma \cos(\phi - \Phi_r + \varepsilon_r) \tag{5.44}$$

Substituting this into the general equation of phase stepping,

$$\tan\phi = \frac{\sum_{r=1}^{R} I_r \sin\Phi_r}{\sum_{r=1}^{R} I_r \cos\Phi_r} \tag{5.45}$$

gives

$$\tan\phi' = \frac{\sum_{r=1}^{R} I'_r \sin\Phi_r}{\sum_{r=1}^{R} I'_r \cos\Phi_r} \tag{5.46}$$

The error in the calculated value of $\phi$ will be

$$\Delta\phi = \arctan\frac{\sum_{r=1}^{R} I'_r \sin\Phi_r}{\sum_{r=1}^{R} I'_r \cos\Phi_r} - \arctan(\tan\phi) \tag{5.47}$$

Assuming that $\varepsilon_r$ is small, it can be shown [**17**] that

$$\Delta\phi = \arctan\left\{\frac{\sum_{r=1}^{R}\varepsilon_r - \sum_{r=1}^{R}\varepsilon_r \cos 2\Phi_r \cos 2\phi - \sum_{r=1}^{R}\varepsilon_r \sin 2\Phi_r \sin 2\phi}{R - \sum_{r=1}^{R}\varepsilon_r \cos 2\Phi_r \sin 2\phi + \sum_{r=1}^{R}\varepsilon_r \sin 2\Phi_r \cos 2\phi}\right\} \tag{5.48}$$

This expression is plotted in figure 5.3 for values of $R$ from 3 to 5. The general trend is that of an error in calculated phase at double the frequency of the phase, *i.e.* at $2\Phi$, centred at approximately $\varepsilon_r$ due to the dominant term $\sum_{r=1}^{R} \varepsilon_r / R$ in the above expression.

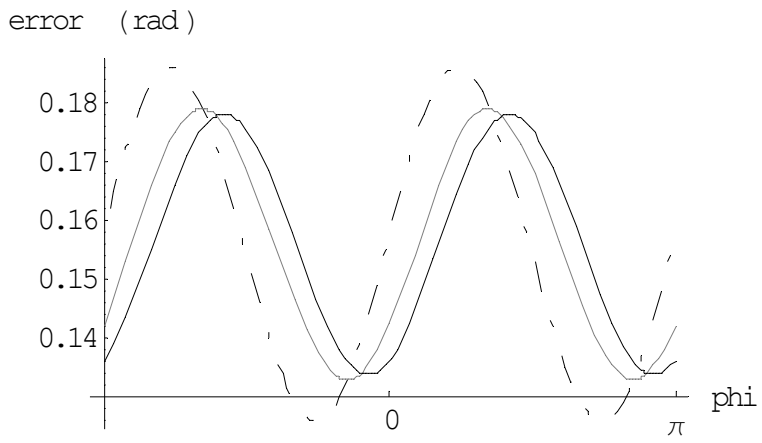


***Figure 5.3*** *- Errors in general 3, 4 and 5-position techniques for phase step error $\varepsilon_r=\pi/20$. The 3, 4 and 5 position techniques are represented by the dashed, dotted and solid lines, respectively*

However for a given value of *R*, this represents a constant offset of the calculated phase which can be removed from the resulting phase map as a constant term. The error at twice the phase frequency is visible as an apparent surface undulation in the phase map. One method of minimising its effect is to increase the number of fringes across the image, and then use smoothing or filtering to remove the high frequency noise from the low frequency surface undulations.

However when measuring long objects, the increase in the number of fringes across the surface amounts to extra tilt of one of the wavefronts. This is an obliquity effect (see § 4.1.2.1) and causes an error in the measured length which is dependent on the length being measured and on the angle of the obliquity effect. Introducing too much tilt may also compromise the detection of the intensity data as the size of each fringe approaches the detector's pixel size.

The analysis of phase-shifting errors, both linear and non-linear, have been simulated by Creath [**3**]. The results of the simulations confirm the $2\Phi$ nature of the error, and show that the greater the number of steps, the lower the amplitude of the error. Thus the techniques of phase-stepping and phase-shifting offer similar accuracies.

One technique to remove the errors introduced by incorrect phase-stepping is to use an additional set of interferograms to directly evaluate the size of each phase-step, using a FFT method [**29**]. This technique offers a repeatability in phase determination to $\lambda/500$ RMS, but requires either a nominally fixed phase-step, taken 8 times (an 8-position technique) or a 10 step technique used with random phase-steps. This technique is also prone to errors with poor fringe contrast or limited detector quantisation range.

Self calibration algorithms often experience problems when there are very few fringes across the image, as the calculations for $\alpha$ and $\phi$ can then contain numerators and denominators close to zero, leading to errors in the arctangent calculation.

### 5.3.7.2 Error due to detector response

A second source of error in the phase calculation is due to the response of the detector used to digitise the interferograms. For all of the techniques examined, it is assumed that the detector has a linear response, *i.e.* the digitised level of fringe intensity, $I_{dig}$, is linearly related to the actual intensity, $I$.

$$I_{dig} = \beta I \tag{5.49}$$

where $\beta$ is a constant. However it is conceivable that for certain detectors, this may not be true, and non-linearities of orders 2, 3, *etc.* may be present.

$$I_{dig} = \beta I + \kappa I^2 + \rho I^3 + \ldots \tag{5.50}$$

Stetson & Brohinski [**30**] have analysed various algorithms and non-linearities, and their results are shown in table 5.3. An asterisk indicates that the non-linearity affects the phase calculation, a blank indicates that the effect of the non-linearity is cancelled in the calculation method. The results for 2nd and 3rd order non-linearities have been confirmed by van Wingerden *et al* [**31**].

| R | 2nd order | 3rd order | 4th order | 5th order | 6th order |
|---|---|---|---|---|---|
| 3 | * | | * | * | |
| 4 | | * | | * | |
| 5 | | | * | | * |

***Table 5.3*** *- Non-linearity effects present for R-step algorithm*

The effect of non-linearities on the phase calculation diminishes with the order of the non-linearity, *i.e.* the effect of a 3rd order non-linearity will be larger than that of a 4th order. The effects of orders greater than 3 are negligible, hence from the above table a minimum of 5 steps should ensure that the effects of detector non-linearities are removed from the phase calculation.

It may be argued that one could use a larger number of phase-steps and completely remove the effects of detector non-linearity, and also achieve greater averaging of the error due to the phase-step error [**29**], however these techniques require much more storage for the digitised images, and longer processing times. The overall resolution of the techniques is limited by vibration, air turbulence, and surface form. PSI is used to measure surface displacements of the order of nanometres, and this is approaching the dimensions of atomic spacings, approximately 0.5 nm. As the number of phase-steps, *R*, is increased, it is difficult to stabilise the measurement system for the longer time necessary for the extra digitisation. Thus it is rarely useful to increase the number of phase steps and complicate matters, when the technique itself is fundamentally limited to approximately *λ/500* to *λ/1000*.

### 5.3.7.3 Error due to multiply-reflected beams

A third possible source of error is due to multiply reflected beams in the interferometer. This produces fringes with a profile similar to those in Fizeau interferometers. Hariharan [**32**] examined the effect of multiply-reflected beams by expanding the classical fringe intensity equation for a Fizeau interferometer.

$$I = I_0\left\lceil \frac{2R(1-\cos\phi)}{1+R^2-2R\cos\phi} \right\rceil \tag{5.51}$$

$$= \frac{2I_0R}{1+R^2}\left\{ \frac{1-\cos\phi}{1-\frac{2R\cos\phi}{1+R^2}} \right\} \tag{5.52}$$

assuming $\frac{2R\cos\phi}{1+R^2}$ is small, then

$$I \approx \frac{2I_0R}{1+R^2}\left\{1-\cos\phi+\frac{2R\cos\phi}{1+R^2}-\frac{2R\cos^2\phi}{1+R^2}\right\} \tag{5.53}$$

$$I = \frac{2I_0R}{1+R^2}\left\{(1-R)-(2R-1)\cos\phi-R\cos 2\phi\right\} \tag{5.54}$$

Inside the brackets, the first term, *(1-R)*, represents the background intensity, the second term represents the *cosϕ* fringes, and the third term appears as extra harmonics of cos*2ϕ*. Note, this expression is only valid for $R << 1$.

For a 3-step technique, Hariharan showed this to introduce a phase error proportional to $\cos\phi \cos 2\phi$, to a first approximation. For $R = 0.05$, the maximum phase error was 6.3°. With a 4-step technique, Hariharan showed the error was reduced to 0.24°. Thus the increased number of digitised images acts as a Fourier filter, removing terms involving $\cos 2\phi$. The Fourier response of a particular 5-step technique are detailed below in § 5.4. Schwider *et al* [**17**] considered the effect of extraneous coherent light at a different phase to the reference and test beams. They showed the error to be periodic in the difference between $\phi$ and the phase of the extraneous light.

Chen & Murata [**33**] demonstrated a phase-stepping Fizeau interferometer, using spatial filtering to remove the effects of multiply-reflected beams, to approximate a sinusoid. Recently Bönsch & Böhme [**34**] have demonstrated a phase-stepping Fizeau algorithm which uses a four-position technique to solve for the 4 unknowns of the Fizeau fringe profile equation. However this technique is prone to discontinuities and errors which depend on the reflectivities of the surfaces and phase stepper accuracy [**35**].

#### 5.3.7.4 Error due to quantisation noise during digitisation

The intensity of the interferogram at each point is sample using a CCD camera and then digitised by an analogue to digital converter. The limited number of quantisation levels of the converter will introduce quantisation noise. The magnitude of the noise will be half of one digitisation level, thus the use of more levels decreases the noise. Van Wingerden *et al* [**31**]have derived a result for the error $\delta\phi$ in calculated phase due to quantisation noise in the digitiser for a generalised phase-stepping technique where $R$ images are used at $N$ bit quantisation with a fringe intensity modulation depth of $m$. Their result is given in equation (5.55).

$$\delta\phi = \frac{1+m}{\sqrt{3R}2^{N+1/2}m} \tag{5.55}$$

For the Primary Length Bar Interferometer which uses an 8 bit digitiser with 5 digitised images of between 0.9 and 1.0 modulation depth, the error in the measured phase is approximately 0.0015 radians (see table 5.4), equivalent to 0.00024 fringe or 0.07 nm.

| N | m = 1 | m = 0.9 | m = 0.5 |
|---|---|---|---|
| 6 (64 levels) | 0.0057 | 0.0060 | 0.0086 |
| 8 (256 levels) | 0.0014 | 0.0015 | 0.0021 |
| 10 (1024 levels) | 0.0004 | 0.0004 | 0.0005 |
| 12 (4096 levels) | 0.0001 | 0.0001 | 0.0001 |

***Table 5.4*** *- Phase measurement error (radians) due to digitisation quantisation noise for an N-bit digitiser with fringes of modulation depth m using a 5-step technique*

## 5.4 AN ERROR-COMPENSATING FIVE POSITION TECHNIQUE

In table 5.3 above, it was seen that a 5-position technique is insensitive to low order detector non-linearities. In the appendix of their paper, Schwider *et al* [**17**] mention a 5-position technique, using phase step values of

$$\Phi_r = 0, \quad \pi/2, \quad \pi, \quad 3\pi/2, \quad 2\pi \tag{5.56}$$

with the phase calculated from

$$\phi = \arctan\left[\frac{2(I_2 - I_4)}{2I_3 - I_5 - I_1}\right] \tag{5.57}$$

for which they estimate an error of size arctan($\varepsilon/2$), where $\varepsilon$ is the phase-step error. However, Hariharan *et al* [**36**] re-calculated the error to be much smaller than this, and the conclusion of van Wingerden *et al* [**31**] is that the 5 position technique is always preferable to the 4 position technique as the measurement errors are the same or better, and the formula takes less computation time.

To analyse these findings it is necessary to derive the 5-position equation. For ease of derivation, assume that the phase steps have relative phases of $-2\alpha$, $-\alpha$, $0$, $\alpha$, $2\alpha$. The intensity at a point in the interferogram can be written as a simple function of the interference of two beams, with the two beam intensities $A$ and $B$, and five intensity values $I_1$ to $I_5$, corresponding to the above phase shifts.

$$\begin{aligned}
I_1 &= A + B + 2\sqrt{AB}\cos(\phi - 2\alpha) \\
I_2 &= A + B + 2\sqrt{AB}\cos(\phi - \alpha) \\
I_3 &= A + B + 2\sqrt{AB}\cos(\phi) \\
I_4 &= A + B + 2\sqrt{AB}\cos(\phi + \alpha) \\
I_5 &= A + B + 2\sqrt{AB}\cos(\phi + 2\alpha)
\end{aligned} \tag{5.58}$$

*i.e.* the reference phase $\Phi_r$ takes values of $-2\alpha$, $-\alpha$, $0$, $\alpha$, $2\alpha$ for $r$ = 1 to 5 respectively.

Then it can be seen that the expression $\dfrac{I_2 - I_4}{2I_3 - I_5 - I_1}$ is equal to

$$\frac{A + B + 2\sqrt{AB}\cos(\phi - \alpha) - A - B - 2\sqrt{AB}\cos(\phi + \alpha)}{2A + 2B + 4\sqrt{AB}\cos(\phi) - A - B - 2\sqrt{AB}\cos(\phi + 2\alpha) - A - B - 2\sqrt{AB}\cos(\phi - 2\alpha)}$$

and then using the sum of angles relation for cosine,

$$\cos(x+y) = \cos(x)\cos(y) - \sin(x)\sin(y)$$

gives

$$\frac{I_2 - I_4}{2I_3 - I_5 - I_1} = \frac{\sin\alpha\sin\phi}{(1 - \cos 2\alpha)\cos\phi} \qquad (5.59)$$

$$= \tan\phi\left(\frac{\sin\alpha}{1 - \cos 2\alpha}\right)$$

The phase step factor $\left(\dfrac{\sin\alpha}{1 - \cos 2\alpha}\right)$ has a value of 0.5 at $\alpha$ = 90° and does not depart from this value for small deviations in $\alpha$ from 90°. If $\alpha$ remains between 86° and 94° then the value of this factor does not alter by more than 0.001 and can be assumed to be constant, see figure 5.4. Assuming a value of 0.5 allows equation (5.59) to be simplified, leading to (5.57).

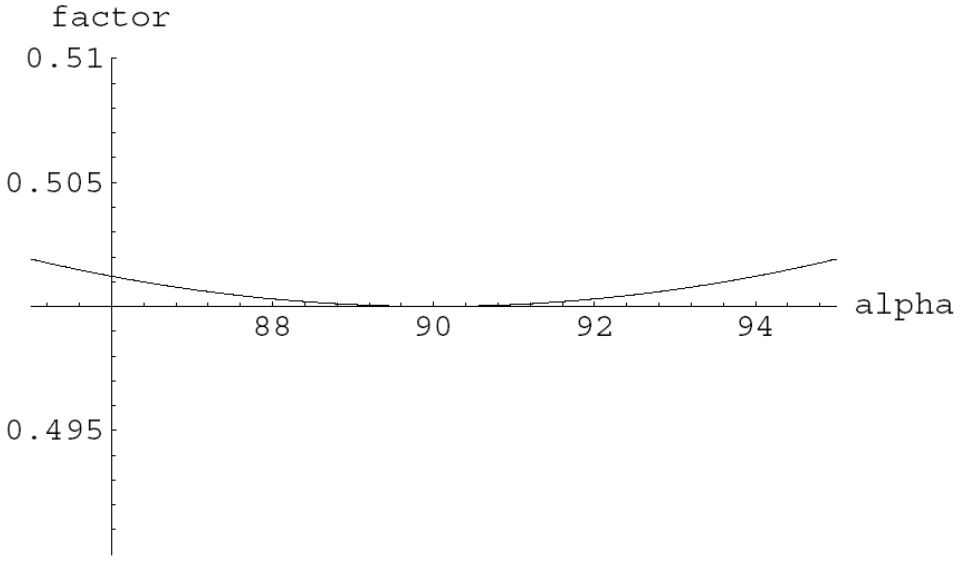


***Figure 5.4*** *- Variation of phase step factor as $\alpha$ is varied*

In fact, if we assume a phase step error of $\varepsilon$, then

$$\alpha = \pi / 2 + \varepsilon \tag{5.60}$$

and

$$\tan \phi' \approx \left(1 + \varepsilon^2 / 2\right) \tan \phi \tag{5.61}$$

$$\Delta\phi = \phi - \phi' = \frac{\varepsilon^2}{4} \sin(2\phi) \tag{5.62}$$

Thus the error in the phase calculation has the expected $2\phi$ dependence, but its magnitude is one quarter of the square of the original phase-step error. As an example, if $\varepsilon = 1°$, then the maximum error $\Delta\phi = 0.02°$. For a double pass interferometer where each fringe corresponds to approximately 316 nm path difference, this amounts to an error in the surface or length measurement of 0.02 nm.

This approximation can be checked by a more rigorous approach.

Assuming $\alpha = \pi/2 + \varepsilon$, then

$$\begin{aligned} I_1 &= A + B + 2\sqrt{AB}\cos(\phi - \pi - 2\varepsilon) \\ I_2 &= A + B + 2\sqrt{AB}\cos(\phi - \pi/2 - \varepsilon) \\ I_3 &= A + B + 2\sqrt{AB}\cos(\phi) \\ I_4 &= A + B + 2\sqrt{AB}\cos(\phi + \pi/2 + \varepsilon) \\ I_5 &= A + B + 2\sqrt{AB}\cos(\phi + \pi + \varepsilon) \end{aligned} \tag{5.63}$$

$$\tan \phi' = \frac{2\left[\cos(\phi - \pi/2 - \varepsilon) - \cos(\phi + \pi/2 + \varepsilon)\right]}{2\cos\phi - \cos(\phi + \pi + \varepsilon) - \cos(\phi - \pi - 2\varepsilon)}$$

$$= \frac{2\left[\sin(\phi - \varepsilon) + \sin(\phi + \varepsilon)\right]}{2\cos\phi + \cos(\phi + 2\varepsilon) + \cos(\phi - 2\varepsilon)} \tag{5.64}$$

$$= \frac{2\sin\phi\cos\varepsilon}{\cos\phi + \cos\phi\cos 2\varepsilon}$$

$$\therefore \ \tan\phi' = \tan\phi\left(\frac{2\cos\varepsilon}{1 + \cos 2\varepsilon}\right) \tag{5.65}$$

For the above phase step error of 1°, this expressions predicts a maximum error in the calculated value of $\phi$ to be 0.05°, similar to the approximate result above.

The expression for arctan $\phi$ (5.57) is such that it is impossible for both the numerator and denominator to be simultaneously zero, with sinusoidal fringes, so no accuracy is lost due to small angle problems.

It is possible to calculate $\alpha$ from the intensity data, allowing a check on the performance of the phase-stepping of the reference mirror:

$$\cos\alpha = \frac{I_5 - I_1}{2(I_4 - I_2)} \tag{5.66}$$

$\alpha$ should have a uniform value of 90° over the measurement surface if the phase-stepping has been performed correctly. Any tilting of the reference mirror during phase-stepping can be identified, as can incorrect calibration of the phase-step size.

Recent work by Larkin and Oreb [**37**] has shown this 5-position technique to be one of a class of 'N+1 symmetrical' techniques. Using Fourier analysis of the effective sampling algorithms, *i.e.* the step positions for which the intensity is digitised, they have shown that the frequency response of the numerator and denominator of equation (5.57) have certain features which make the algorithm insensitive to certain errors:

- The numerator has stationary points at the fundamental fringe frequency, and at odd-multiples of this frequency. Thus, at these frequencies, the numerator is insensitive to phase-step errors (which produce a frequency slightly different to the fundamental frequency).

- The numerator also has zeroes at all even-multiples of the fundamental frequency, making it insensitive to even-order detector non-linearities.

- The denominator has stationary points at the fundamental frequency and all multiples. Thus the denominator is insensitive to phase-step errors.

- The denominator also has zeroes at the even-harmonics, and hence is not affected by even-order detector non-linearities.

Hence the overall technique is insensitive to even-order detector non-linearities and phase-step errors, particularly those close to the fundamental fringe frequency, *i.e.* small phase-step errors, as demonstrated above in figure 5.4. It is simple to implement and provides a self-check of attained phase-step values.

## 5.5 IMPLEMENTATION OF THE FIVE POSITION TECHNIQUE IN THE PRIMARY INTERFEROMETER

Due to the advantages summarised above, the 5 position technique was chosen for use in the analysis of the interference patterns in the Primary Length Bar Interferometer. A phase-step of size $\pi/2$ is provided by moving the mirror in the reference arm of the interferometer by 1/4 of a fringe (at $\lambda$ = 633 nm , this is equal to 79 nm). Problems of incorrect phase-stepping have been overcome by design of the mirror mount (see § 3.2.3), and by using a commercial PZT system which uses capacitive sensing to maintain the PZT calibration. The PZT can be moved in steps of size 1.07 nm by setting the digital offset in the control electronics by computer control.

The phase-stepping is performed as follows. Firstly the PZT is positioned at the centre of its range (digital offset = 0). The red laser is selected. After a 2 second pause, the image is digitised. The PZT is moved to the next position (offset = 74), and allowed to stabilised for 0.25 sec before the 2nd image is captured. The PZT is then moved to the 3rd position (offset = 148) and stabilised before the image is captured. This is repeated until 5 images have been digitised for the red wavelength.

The red laser is de-selected, the green laser selected and the PZT positioned back at the starting position. The process of digitising the image, moving the mirror, stabilising, *etc.* is repeated for the green wavelength and then for the orange wavelength.

The size of each step is adjusted for the wavelength being used. The whole 3-wavelength phase-stepping procedure lasts approximately 7 seconds.

Equation (5.66) is used to calculate the exact phase step at each non-masked pixel, and the average of the values from all non-masked pixels provides a check on the calibration of the PZT movement and the accuracy of the phase-stepping. Any tilt of the mirror during stepping can be seen in the $\alpha$ map as a change in phase step angle. In practice the phase-stepping is very reliable and usually phase-step correction is unnecessary. Average phase step sizes are 90° ± 2°, leading to a maximum phase measurement error of 0.06° or 0.05 nm.

**REFERENCES FOR CHAPTER 5**

[**1**] Brown G M Fringe analysis for automotive applications Proceedings of conference Fringe Analysis '92, Leeds 1992, (London: Institute of Physics)

[**2**] Ascough J Applications of three-dimensional photoelasticity in hip joint prosthesis design *Proceedings of conference Fringe Analysis '92*, Leeds 1992, (London: Institute of Physics)

[**3**] Creath K Phase measurement interferometry techniques *Progress in Optics* (Elsevier: North Holland) **26** (1988) 349-393

[**4**] Hariharan P Optical Interferometry *Rep. Prog. Phys.* **54** (1991) 339-390

[**5**] Hariharan P Interferometry with lasers *Progress in Optics* (Elsevier: North Holland) **24** (1987) 103-164

[**6**] Reid G T Automatic fringe pattern analysis: a review *Optics and Lasers in Engineering* **7** (1986) 37-68

[**7**] Robinson D W Automatic fringe analysis in optical metrology *Appl. Opt.* **22** (1983) 2169-2176

[**8**] Schwider J Advanced evaluation techniques in interferometry *Progress in Optics* (Elsevier: North Holland) **28** (1990) 217-359

[**9**] Budzinski J SNOP: a method for fringe skeletonization of a fringe patern along a fringe direction *Appl. Opt.* **31** (1992) 3109-3113

[**10**] Parthiban V & Sirohi R S Interactive fringe procesing algorithm for interferogram analysis *Optics and Lasers in Engineering* **11** (1989) 103-113

[**11**] Hou W & Wilkening G Investigation and compensation of the nonlinearity of heterodyne interferometers *Precis. Eng*. **14** (1992) 91-98

[**12**] Takeda M Spatial-carrier fringe-pattern analysis and its applications to precision interferometry and profilometry: an overview *Industrial Metrology* **1** (1990) 79-99

[**13**] Carré P Installation et utilisation du comparateur photoélectrique et interférential du Bureau International des Poids et Mesures *Metrologia* **2** (1966) 13-23

[**14**] Bruning J H, Herriott D R, Gallagher J E, Rosenfeld D P, White A D & Brangaccio D J Digital wavefront measuring interferometers for testing optical surfaces and lenses *Appl. Opt.* **13** (1974) 2693-2703

[**15**] Sommargren G E Optical heterodyne profilometry *Appl. Opt.* **20** (1981) 610-618

[**16**] Wyant J C Use of an ac heterodyne lateral shear interferometer with real-time wavefront corection systems *Appl. Opt.* **14** (1975) 2622-2626

[**17**] Schwider J, Burow R, Elssner K E, Grzanna R, Spolaczyk R & Merkel K Digital wavefront measuring interferometry: some systematic error sources *Appl. Opt.* **22** (1983) 3421-3432

[**18**] Grievenkamp J E Generalized data reduction for heterodyne interferometry *Opt. Eng.* **23** (1984) 350-352

[**19**] Cheng YY & Wyant J C Two wavelength phase shifting interferometry *Appl. Opt.* **23** (1984) 4539-4543

[**20**] Pettyjohns K N, De Vore S, Deraniak E & Wyant J C Direct phase measurement interferometer working at 3.8 μm *Appl. Opt.* **24** (1985) 2211-2216

[**21**] Creath K Step height measurement using two-wavelength phase-shifting interferometry *Appl. Opt.* **26** (1987) 2810-2816

[**22**] Barnes T H Heterodyne Fizeau interferometer for testing optical flats *Appl. Opt.* **26** (1987) 2804-2809

[**23**] Srinivasan V, Liu H C & Halioua M Automated phase measuring profilometry of 3D diffuse objects *Appl. Opt*. **23** (1984) 3105-3108

[**24**] Shagam R N & Wyant J C Optical frequency shifter for heterodyne interferometers using multiple rotating polarisation retarders *Appl. Opt.* **17** (1978) 3034-3035

[**25**] Colucci D & Wizinowich P Millisecond phase acquisition at video rates *Appl. Opt.* **31** (1992) 5919-5925

[**26**] Kothiyal M P & Delisle C Rotating analyzer heterodyne interferometer: error sources *Appl. Opt.* **24** (1985) 2288-2290

[**27**] Grievenkamp J E Generalized data reduction for heterodyne interferometry *Opt. Eng.* **23** (1984) 350-352

[**28**] Santoyo F M, Kerr D & Tyrer J R Interferometric fringe analysis using a single phase step technique *Appl. Opt.* **27** (1988) 4362-4364

[**29**] Lai G & Yatagai T Generalized phase-shifting interferometry *J. Opt. Soc. Am.* **A8** (1991) 822-827

[**30**] Stetson K A & Brohinski W R Electooptic holography and its application to hologram interferometry *Appl. Opt*. **24** (1985) 3631-3637

[**31**] van Wingerden T, Frankena H J, Smorenburg C Linear approximation for measurement errors in phase shifting interferometry *Appl. Opt*. **30** (1991) 2718-2729

[**32**] Hariharan P Digital phase-stepping interferometry: effects of multiply reflected beams *Appl. Opt*. **26** (1987) 2506-2507

[**33**] Chen J & Murata K Digital phase measuring Fizeau interferometer for testing of flat and spherical surfaces *Optik* **81** (1988) 28-32

[**34**] Bönsch G & Böhme H Phase-determination of Fizeau interferences by phase-shifting interferometry *Optik* **82** (1989) 161-164

[**35**] Nicolaus R A Evaluation of Fizeau interferences: a comparison of phase-stepping algorithms *Proc. SPIE* **1319** (1990) 237-238

[**36**] Hariharan P, Oreb B F & Eiju T Digital phase-shifting interferometry: a simple error-compensating phase calculation algorithm *Appl. Opt.* **26** (1987) 2504-2505

[**37**] Larkin K G & Oreb B F Design and assessment of symmetrical phase-shifting algorithms *J. Opt. Soc. Am.* **A9** (1992) 1740-1748